Electronic distributions of states in crystalline and quasicrystalline Al-Cu-Fe and Al-Cu-Fe-Cr

alloys

Electronic distributions of states in crystalline and quasicrystalline Al–Cu–Fe and Al–Cu–Fe–Cr alloys

Esther Belin†, Zoltan Dankhazi‡, Anne Sadoc§, Yvonne Calvayrac‖, Thierry Klein¶ and Jean-Marie Dubois††

† Laboratoire de Chimie Physique, Matière et Rayonnement (Unité associée au CNRS 176), 11 rue Pierre et Marie Curie, 75231 Paris Cédex, France
‡ Laboratory of Surface and Interface Physics, Eötvos University, Muzéum krt. 6-8 H-1088 Budapest, Hungary
§ Laboratoire d'Utilisation du Rayonnement Electromagnétique (CNRS, CEA, MENJS), Bâtiment 209D, Université Paris-Sud, 91405 Orsay Cédex, France
‖ Centre d'Etudes de Chimie Métallurgique (CNRS), 15 rue Georges Urbain, 94407 Vitry Cédex, France
¶ Laboratoire d'Etudes des Propriétés Electroniques des Solides (CNRS), BP 166X, 38042 Grenoble Cédex, France
†† Laboratoire des Sciences et Genie des Matériaux Métalliques (Unité associé au CNRS 159), Parc de Saurupt, 54042 Nancy Cédex, France

Abstract. Valence and conduction state distributions in a series of Al–Cu–Fe and Al–Cu–Fe–Cr alloys of different structural states and nominal compositions have been investigated by means of soft-x-ray emission and photoabsorption spectroscopies. A complete description of the valence band is obtained. The DOS at E_F is observed to be very low which is consistent with the high resistivity values found for the icosahedral quasicrystalline phase. The existence of a wide pseudo-gap at E_F is evidenced, which is higher in the quasicrystal than in the related crystalline counterparts.

1. Introduction

In recent years, several papers have been devoted to the experimental study of the electronic properties of different quasicrystalline phases (see, e.g., Wagner *et al* 1989, Matsuo *et al* 1989, Biggs *et al* 1990, Berger *et al* 1991, Phillips and Rabe 1991). At the same time, interest is increasing in the theoretical determination of the electronic structure of these alloys and several calculations have been performed for appropriate crystalline approximants of the quasicrystalline phases (see, e.g., Fujiwara and Yokokawa 1991). The electronic properties of quasicrystals composed of sp materials show similarities to related metallic glasses. For Al–Cu–Fe quasicrystals, which because of their particular stability are going to be extensively studied, the extremely high resistivities observed for $Al_{65}Cu_{23}Fe_{12}$ and for $Al_{62.5}Cu_{25}Fe_{12.5}$ (Klein *et al* 1990, 1991) are interpreted as a consequence of the low density of states (DOS) at E_F (Kimura *et al* 1991). Therefore, the understanding of the properties could be improved if one could investigate the *electronic distributions* and obtain insight into *how they are interacting in these materials*. This is the question that we are going to try to answer.

In previous papers we have already focused on the experimental determination, by means of the soft-x-ray spectroscopy (SXS) technique, of both valence and conduction DOSs in a series of Al–Mn-based alloys; these samples were in several structural states, namely crystalline, amorphous and quasicrystalline (Traverse *et al* 1988, Belin and Traverse 1991, Belin *et al* 1991). The results evidenced clearly the occurrence of a pseudo-gap opening at E_F in the Al DOS; the gap width becomes larger as the Mn content increases in the alloy whatever the structural state might be and it is wider for a quasicrystal than for a crystal at a given Mn concentration. The Mn 3d and Al 3sp valence states interact near E_F over a few electron-volts; then, towards increasing binding energies, the states are Al 3sp and then almost pure Al 3s.

We have extended these analyses to a series of stable Al–Cu–Fe and Al–Cu–Fe–Cr quasicrystalline alloys and their related crystalline phases. In the present paper, we report an experimental study of the valence band DOS and of the unoccupied p DOS. Here also, we have used the SXS technique. Indeed, it is well known that SXS experiments allow one to investigate separately occupied (soft-x-ray emission spectroscopy (SXES) experiments) and unoccupied (soft-x-ray photoabsorption spectroscopy (SXAS) experiments) DOSs. Owing to the dipole matrix element, which is involved in radiative transition probabilities, the electronic distributions of a selected angular momentum around each of the various components of the solid can be obtained separately. The information which we shall report here concerns the bulk material.

The paper is organized as follows: in section 2 we describe briefly the experimental procedures and the samples that we have used; the results are presented and detailed in section 3. The last section is dedicated to the discussion of all the data; a complete picture of the valence band states distribution is thus proposed.

2. Experimental procedure

Table 1 indicates the different spectra which we have analysed to obtain the valence and conduction state distributions. This table does not mention Cr because no reliable Cr $L\alpha$ spectrum could be obtained in our experimental conditions owing to poor resolution and intensity in the energy range of this x-ray transition.

Table 1. Experimental parameters: VB, valence band; CB, conduction band.

SXS line	Transition	Valence states	Conduction states	Crystal or grating	Energy resolution (eV)	Energy range (eV)
Al Kβ	1s←VB	3p		SiO$_2$ 10$\bar{1}$0	0.2	1545–65
Al L$_{2,3}$	2p←VB	3s		Grating	0.3	60–67
Fe Lα	2p$_{3/2}$ ←VB	3d–4s		RbAP	0.3	700–10
Cu Lα	2p$_{3/2}$ ←VB	3d–4s		RbAP	0.3	920–35
Al K	1s→CB		p	SiO$_2$	0.5	1555–65
Fe K	1s→CB		p	SiO$_2$	0.5	7100–15
Cu K	1s→CB		p	SiO$_2$	0.5	8970–85

The measurements were carried out by means of various experimental set-ups. The SXES experiments were performed with Johann-type vacuum spectrometers equipped with either a grating of 600 grooves mm^{-1} bent with a radius of 2 m or with

a RbAP or SiO_2 ($10\bar{1}0$) crystal bent with a radius of 0.5 m. These spectrographs were fitted with electronic detection equipment and the spectra were scanned by successive steps along the Rowland cylinder of the grating or crystals. The sample was used as the target of the x-ray tube; it was glued on a water-cooled holder by means of silver glue. The spectra were produced by electro-excitation for Al $K\beta$ and Al $L_{2,3}$ bands and photon excitation for Fe and Cu $L\alpha$ bands. This means that oxide contribution to the spectra can be present in the former case. The photoabsorption measurements were carried out at the Laboratoire d'Utilisation du Rayonnement Electromagnétique (LURE). Super ACO storage ring with a two-quartz-crystal monochromator or DCI facility equipped with a Si 331 channel cut monochromator were used (Sadoc *et al* 1991).

The experimental energy resolutions and the spectral ranges that were investigated are also reported in table 1.

Table 2. Structural states of the experimented Al–Cu–Fe and Al–Cu–Fe–Cr alloys that were studied.

Sample	Structural state
$Al_{46}Cu_{36}Fe_{18}$	Crystalline
$Al_{55}Cu_{33}Fe_{12}$	Crystalline
$Al_{62}Cu_{25.5}Fe_{12.5}$, as quenched	Icosahedral
$Al_{62}Cu_{25.5}Fe_{12.5}$, annealed	Icosahedral
$Al_{65.5}Cu_{18.5}Fe_8Cr_8$	Icosahedral
$Al_{65.5}Cu_{18.5}Fe_8Cr_8$	Decagonal
$Al_{65.5}Cu_{18.5}Fe_8Cr_8$	Microcrystalline

Table 2 gives a list of the samples that we have investigated and specifies what their structure is: crystalline (C), microcrystalline (μC) and quasicrystalline (QC), i.e. icosahedral (I) or decagonal (D). These samples are all single phase; they were prepared and characterized as described elsewhere (Bessière *et al* 1991, Dong and Dubois 1991, Klein *et al* 1991).

To allow for the adjustment of the different spectra obtained in various energy ranges, we performed complementary determinations. First, we measured the Al, Cu and Fe $2p_{3/2}$ binding energies in the alloys; a Kratos photoemission spectrograph fitted with a Mg anode was used. Charging effects of the samples have been accounted for by calibrating, in each case, the energy scale with respect to C 1s taken as 285.0 eV. The accuracy of the measurements was not better than 0.1 eV for Al and 0.3 eV for Cu or Fe. Second, we also measured the SXES Al $K\alpha_{1,2}$ line ($1s \leftarrow 2p_{3/2,1/2}$) using a beryl crystal bent with a radius of 0.5 m. Within the limits of the experimental precision, the Al $K\alpha_{1,2}$ line wavelength was the same in pure Al and in the alloys.

3. Results

The experimental curves have been adjusted on the binding energy scale where E_F is taken as origin. This adjustment was possible owing to the measurement of, firstly, the $2p_{3/2}$ level energies for Al, Cu and Fe in the alloys as reported in the previous section and secondly, the energy of the transition Al($1s \leftarrow 2p_{3/2,1/2}$) which allows

one to determine the value for the energy of the Al 1s level. As the $2p_{3/2}$ and 1s binding energies are referred to the Fermi level we could locate E_F on the x-ray transition energy scale of each emission spectrum. We have not obtained values for the energies of the Cu 1s and Fe 1s levels in the alloys; we made the assumption that the energy shift of the 1s level is the same as that of the $2p_{3/2}$ levels in these alloys with respect to the pure metals. Then, it was also possible to locate E_F on different SXAS energy scales.

Thus, from these adjustments, it becomes possible to perform a direct comparison of the various experimental electronic distributions on the same energy scale.

The Al Kβ emission bands were corrected for oxide contribution. This could not be done for the Al $L_{2,3}$ band; as a consequence, the shape of these curves is less significant in the energy range of the Al $L_{2,3}$ emission in Al_2O_3. Let us recall that an oxide contribution is not expected for Fe and Cu Lα bands.

The different emission curves are normalized to the same height between their maxima and the wings on each side of the maximum where the variation in intensity is negligible; for Al Kβ, because of the presence of an important tail towards high binding energies, the normalization is made between the maximum and the intensity at about $E_F - 2$ eV.

The photoabsorption curves are normalized between the bottom before the edge (the variation in intensity is negligible) and the intensity beyond the edge, respectively, at about 5 eV for Al K (in this case, no significant oxide contribution can exist) and about 8 eV for Fe K and Cu K.

Figure 1, curves a, b, c, d, e, f and g, are the curves corresponding to the Al 3p distributions in pure Al, in C-$Al_{46}Cu_{36}Fe_{18}$, C-$Al_{55}Cu_{33}Fe_{12}$, I-$Al_{62}Cu_{25.5}Fe_{12.5}$, μC-$Al_{65.5}Cu_{18.5}Fe_8Cr_8$, D-$Al_{65.5}Cu_{18.5}Fe_8Cr_8$ and I-$Al_{65.5}Cu_{18.5}Fe_8Cr_8$, respectively.

The principal maximum A of all the curves, situated at about $+2.5$ eV, is shifted towards high binding energies with respect to pure Al whose maximum is at 1.4 ± 0.1 eV. For C-$Al_{46}Cu_{36}Fe_{18}$ and C-$Al_{55}Cu_{33}Fe_{12}$ alloys, the maximum A is split into two parts. This splitting is not marked for the μC-$Al_{65.5}Cu_{18.5}Fe_8Cr_8$ phase; the whole peak A is set back from the edge towards high binding energies and the edge appears to be doubled; the second slope is located at about $E_F + 1.2$ eV and it is labelled as s on the curves. The structure s is also observed, in the same energy range, in the curve corresponding to sample D-$Al_{65.5}Cu_{18.5}Fe_8Cr_8$; it is not present for the I-$Al_{65.5}Cu_{18.5}Fe_8Cr_8$ nor for the I-$Al_{62}Cu_{25.5}Fe_{12.5}$ phase; in these cases, the edge gently bends towards high binding energies after about $E_F + 1.5$ eV.

A secondary maximum B is observed at about $E_F + 5$ eV in figure 1, curves b–d; in figure 1, curves e–g, this maximum is seen as a shoulder. A faint feature C is also present on all the curves at about $E_F + 7$ eV. With respect to pure Al, because of the existence of peak B, the full width at half-maximum (FWHM) of the Al Kβ band is broadened in Al–Cu–Fe alloys whereas shoulder B does not modify significantly the FWHM of the Al Kβ band in the Al–Cu–Fe–Cr phases.

The intensity at E_F varies from one sample to another. For pure Al, the valence band edge cuts E_F at its half-maximum intensity. This is not the case for the alloys. We measure the energy separation to E_F which we take at half-maximum intensity of the emission curves and label it as δ; δ increases with decreasing intensity at E_F. In the I-Al–Cu–Fe alloys, with respect to the crystalline phases, δ increases but the Al concentration is lower in the latter samples. All the same, δ increases from the 'as-quenched' icosahedral sample to the 'annealed' sample; note that in the latter case the diffraction pattern was that of a 'pure quasicrystal' (Calvayrac *et al* 1990). For the
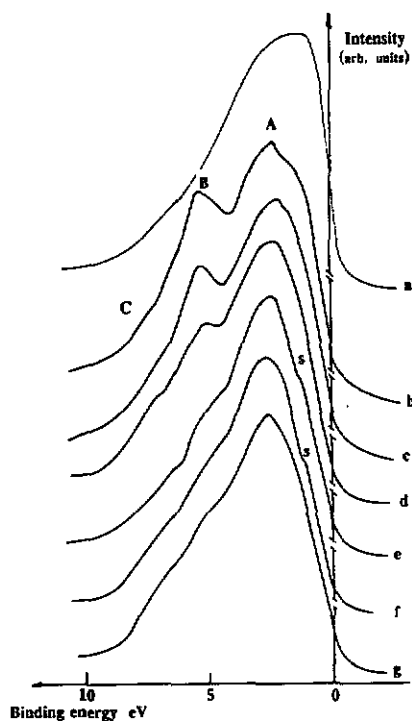
Figure 1. Al 3p state distribution curves: curve a, pure Al; curve b, C-Al$_{46}$Cu$_{36}$Fe$_{18}$; curve c, C-Al$_{55}$Cu$_{33}$Fe$_{12}$; curve d, I-Al$_{62}$Cu$_{25.5}$Fe$_{12.5}$; curve e, μC-Al$_{65.5}$Cu$_{18.5}$Fe$_8$Cr$_8$; curve f, D-Al$_{65.5}$Cu$_{18.5}$Fe$_8$Cr$_8$; curve g, I-Al$_{65.5}$Cu$_{18.5}$Fe$_8$Cr$_8$.

Al–Cu–Fe–Cr alloys, the intensity at E_F is slightly decreased from the microcrystalline to the quasicrystalline phase; in these series of alloys the nominal Al concentration is the same. In a parallel way, one observes that the slope of the emission edge bends progressively towards high binding energies from Al to the alloys and from the crystalline to the quasicrystalline phase. All the data concerning the Al Kβ emission spectra are collected in table 3.

Table 3. Al 3p distributions: energies and intensities of the different structures of the curves, distances to the Fermi level at half-maximum and FWHMs for the Al–Cu–Fe and Al–Cu–Fe–Cr alloys. Data for pure Al are also reported. All values in electron-volts are ±0.1 eV; intensities are ±1.

Alloy	A (eV)	B (eV)	C (eV)	Intensity of B	Intensity at E_F	δ (eV)	FWHM (eV)
C-Al$_{46}$Cu$_{36}$Fe$_{18}$	2.2	5.2	7.3	80	21	0.4	5.9
C-Al$_{55}$Cu$_{33}$Fe$_{12}$	2.4	5.3	7.2	75	21	0.45	5.9
I-Al$_{62}$Cu$_{25.5}$Fe$_{12.5}$ [a]	2.3	5.2	7.4	65	14	0.7	5.6
I-Al$_{62}$Cu$_{25.5}$Fe$_{12.5}$ [b]	2.2	5.1	7.6	70	12	0.7	5.6
μC-Al$_{65.5}$Cu$_{18.5}$Fe$_8$Cr$_8$	2.4	5.2	7.0	56	13	0.8	4.7
D-Al$_{65.5}$Cu$_{18.5}$Fe$_8$Cr$_8$	2.6	5.1	7.2	56	12	0.9	5.0
I-Al$_{65.5}$Cu$_{18.5}$Fe$_8$Cr$_8$	2.5	5.2	7.4	57	11	0.85	5.0
Al	1.4				50		5.0

[a] As quenched
[b] Annealed

Figures 2(*a*) and 2(*b*) show the Al $L_{2,3}$ bands of Al, C-Al$_{55}$Cu$_{33}$Fe$_{12}$, I-Al$_{62}$Cu$_{25.5}$Fe$_{12.5}$, μC-Al$_{65.5}$Cu$_{18.5}$Fe$_8$Cr$_8$, D-Al$_{65.5}$Cu$_{18.5}$Fe$_8$Cr$_8$ and I-Al$_{65.5}$Cu$_{18.5}$Fe$_8$Cr$_8$. As detailed above, the curves are adjusted to the Fermi level. Curve a' in figure 2 which corresponds to the oxide Al$_2$O$_3$ is given on the x-ray transition energy scale. This allows one to locate the ranges where the oxide contribution affects the shape of the Al $L_{2,3}$ emission in the alloys and consequently the intensity of the curves.
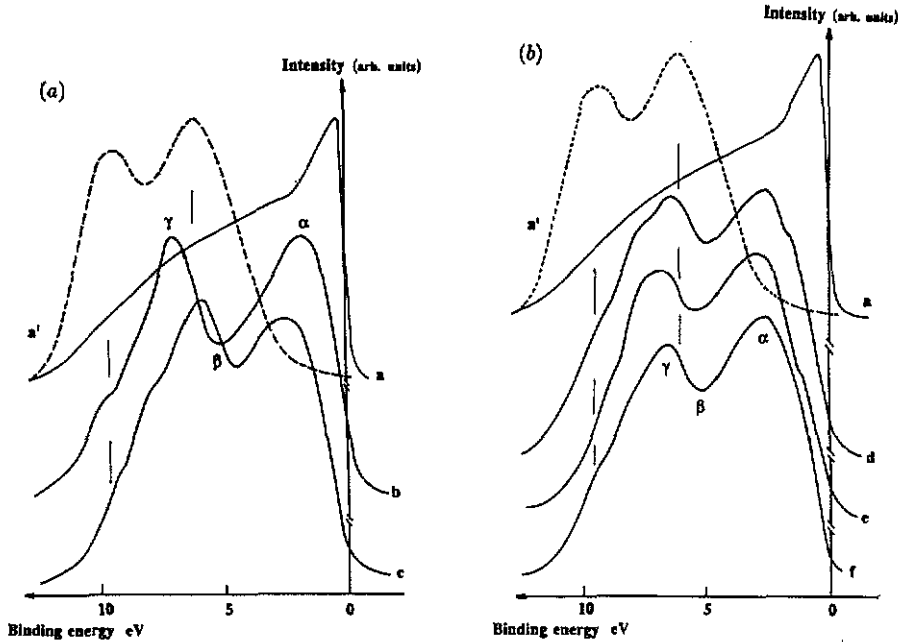

Figure 2. (*a*) Al 3s state distribution curves; curve a, pure Al; curve b, C-Al$_{55}$Cu$_{33}$Fe$_{12}$; curve c, I-Al$_{62}$Cu$_{25.5}$Fe$_{12.5}$; curve a', Al$_2$O$_3$. (*b*) Al 3s state distribution curves; curve a, Al; curve d, μC-Al$_{65.5}$Cu$_{18.5}$Fe$_8$Cr$_8$; curve e, D-Al$_{65.5}$Cu$_{18.5}$Fe$_8$Cr$_8$; curve f, I-Al$_{65.5}$Cu$_{18.5}$Fe$_8$Cr$_8$. The curve of the Al 3s distribution in Al$_2$O$_3$ is shown as a broken curve; the positions of the maxima are shown by vertical bars.

For pure Al, the Al $L_{2,3}$ band is parabola like except near the Fermi level where the distribution shows a strong narrow peak; this peak has been interpreted by several workers as not arising from the DOS but as involving a many-body effect. The curves corresponding to the alloys exhibit a double wide-peaked structure; the intensity of the low-lying peak is not affected by oxidation. The two peaks labelled α and γ are separated by a more or less deep minimum β at about $E_F + 5$ eV. As observed for the Al 3p distributions, the edges of the μC- and D-Al$_{65.5}$Cu$_{18.5}$Fe$_8$Cr$_8$ phases are double stepped; the second part of the edge starts at about $E_F + 1.5$ eV and $E_F + 1.2$ eV for the μC and D alloys, respectively. For the different samples, the intensities at E_F and δ, which are reported in table 4, are the same as those measured for the Al 3p state distributions within the limits of the experimental precision.

The Fe Lα and Cu Lα curves of the alloys are very similar to those of the pure metals. Their FWHMs are decreased by about 0.7–0.9 eV for Fe and 0.1–0.4 eV for Cu; the trend is to decrease slightly from crystalline to quasicrystalline phases. The maxima of the Fe Lα subbands are little changed while those of the Cu Lα are

Table 4. Al 3s distributions: distances from the Fermi level of maximum α and at half-maximum. Data for pure Al are also reported. All values in electron-volts are ± 0.1 eV; intensities are ± 1.

Alloy	α (eV)	Intensity at E_F	δ (eV)
C-Al$_{55}$Cu$_{33}$Fe$_{12}$	1.8	23	0.4
I-Al$_{62}$Cu$_{25.5}$Fe$_{12.5}$[a]	2.8	14	0.8
μC-Al$_{65.5}$Cu$_{18.5}$Fe$_8$Cr$_8$	2.6	12	0.7
D-Al$_{65.5}$Cu$_{18.5}$Fe$_8$Cr$_8$	2.5	12	0.9
I-Al$_{65.5}$Cu$_{18.5}$Fe$_8$Cr$_8$	2.6	11	0.8
Al	0.4	50	0

[a] As quenched.

shifted by about 2 eV towards increased binding energies. All the data corresponding to these spectra are reported in table 5.

Table 5. Fe and Cu 3d–4s distributions: FWHM and distances Δ from the Fermi level of the maximum of the distribution in the pure metals and the Al–Cu–Fe and Al–Cu–Fe–Cr alloys. All values in electron-volts are ± 0.1 eV.

Alloy	Fe FWHM (eV)	Fe Δ (eV)	Cu FWHM (eV)	Cu Δ (eV)
Fe	3.2	2.3		
Cu			3.9	2.8
C-Al$_{55}$Cu$_{33}$Fe$_{12}$	2.4	1.3	3.4	4.1
I-Al$_{62}$Cu$_{25.5}$Fe$_{12.5}$[a]	2.5	1.3	3.7	4.1
μC-Al$_{65.5}$Cu$_{18.5}$Fe$_8$Cr$_8$	2.3	1.35	3.5	4.2
D-Al$_{65.5}$Cu$_{18.5}$Fe$_8$Cr$_8$	2.4	1.2	3.8	4.2
I-Al$_{65.5}$Cu$_{18.5}$Fe$_8$Cr$_8$	2.5	1.4	3.8	4.2

[a] As quenched.

The curves of the Al, Fe and Cu p empty-state distributions in I-Al$_{62}$Cu$_{25.5}$Fe$_{12.5}$ are shown in figure 3 compared with the experimental and theoretical curves for the pure metal. The Al p and Fe p curves are $\tan^{-1}$ like followed by a monotonic increase in intensity; they are almost not changed with respect to those for pure Al or Fe. The Cu K curve for the alloy also increases monotonically whereas, for the metal, there is a slight hollow after the edge followed by a monotonic increase in intensity.

4. Discussion

4.1. Valence band state distributions

Figure 4(a) shows the Al Kβ and Al L$_{2,3}$ bands for C-Al$_{46}$Cu$_{36}$Fe$_{18}$ adjusted to E_F as described above. The two curves overlap over all the experimented energy
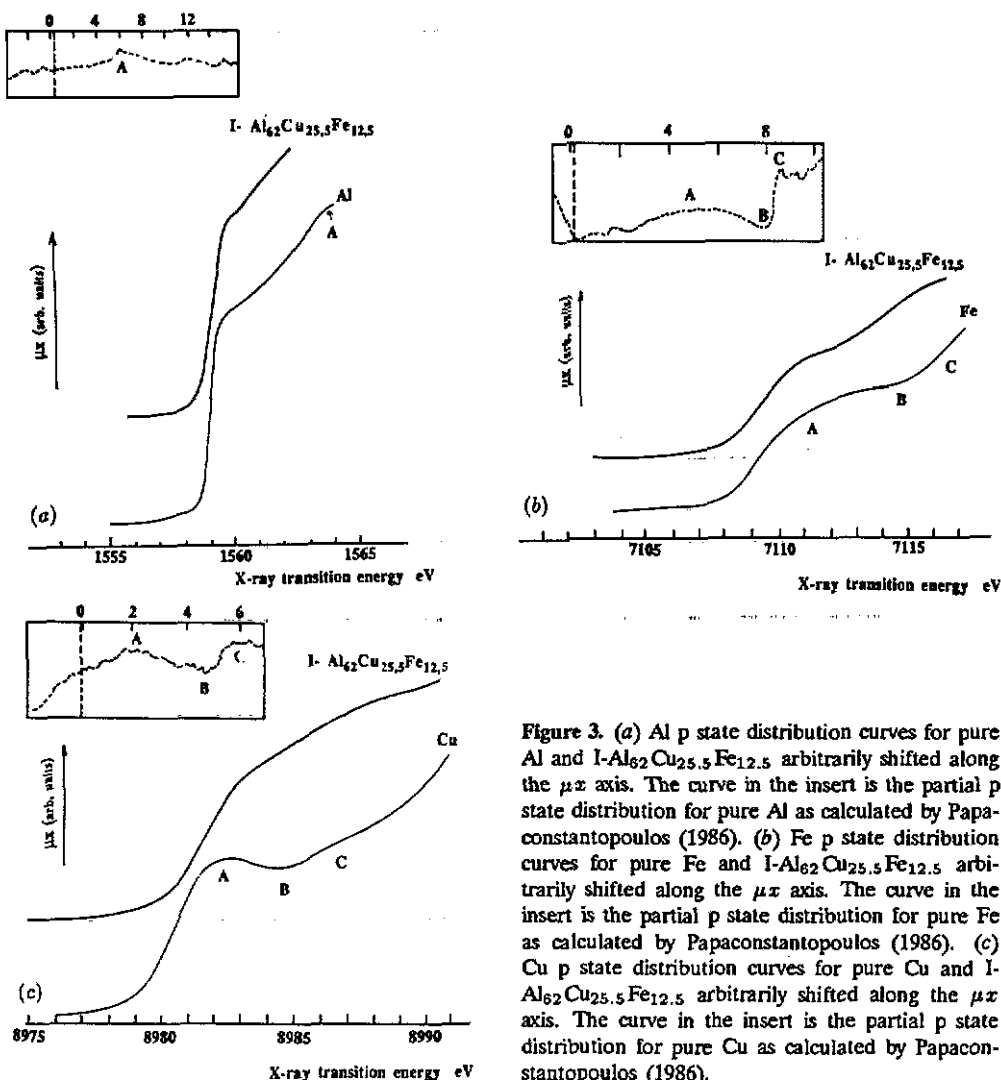
Figure 3. (a) Al p state distribution curves for pure Al and I-Al$_{62}$Cu$_{25.5}$Fe$_{12.5}$ arbitrarily shifted along the μx axis. The curve in the insert is the partial p state distribution for pure Al as calculated by Papaconstantopoulos (1986). (b) Fe p state distribution curves for pure Fe and I-Al$_{62}$Cu$_{25.5}$Fe$_{12.5}$ arbitrarily shifted along the μx axis. The curve in the insert is the partial p state distribution for pure Fe as calculated by Papaconstantopoulos (1986). (c) Cu p state distribution curves for pure Cu and I-Al$_{62}$Cu$_{25.5}$Fe$_{12.5}$ arbitrarily shifted along the μx axis. The curve in the insert is the partial p state distribution for pure Cu as calculated by Papaconstantopoulos (1986).

range, i.e. about 12 eV. The edges of the two subbands are superposed within the experimental precision whatever the alloy is; this means that the corresponding states are completely sp hybridized. With increasing binding energy, one finds first that maxima A of Al Kβ and α of Al L$_{2,3}$ are superposed, second that the peak B of Al Kβ is at the same energy range as minimum β of Al L$_{2,3}$ and finally that the second maximum γ of Al L$_{2,3}$ is on the shoulder C of Al Kβ (note that the vertical bars show the position of the maxima of the Al L$_{2,3}$ band in the oxide). It follows thus that the Al states are sp hybridized from E_F to $E_F + 3$ eV, then almost pure p at around $E_F + 5$ eV and, in the high-lying part, almost pure s because of a faint hybridization with p states.

Let us now adjust the Fe and Cu Lα curves to the Al Kβ and Al L$_{2,3}$ curves. Figure 4(b) displays the result for C-Al$_{55}$Cu$_{33}$Fe$_{12}$. This demonstrates that near E_F the Al curve edges overlap with Fe Lα while the Cu Lα is superposed on the
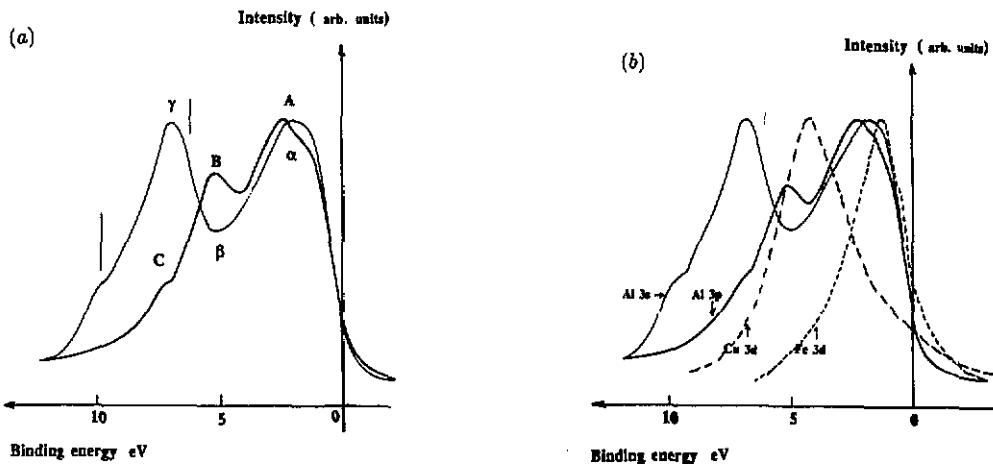
Figure 4. (*a*) Al 3p (bold curve) and Al 3s (thin curve) state distribution curves for C-Al$_{46}$Cu$_{36}$Fe$_{18}$. The vertical bars show the positions of the maxima of the Al 3s distribution in Al$_2$O$_3$. (*b*) Al 3p (bold curve), Al 3s (thin curve), Fe 3d (short dashed curve) and Cu 3d (long dashed curve) state distribution curves for C-Al$_{55}$Cu$_{33}$Fe$_{12}$ alloy.

minimum between peaks A and B of the Al Kβ band.

So, from E_F towards increasing binding energies, the whole valence band is organized as follows.

(i) At E_F, Al, Fe and Cu states are present and the Al DOSS are quite low.

(ii) The edge of the band is Al 3sp interacting with Fe 3d states.

(iii) The states at about 2.5 eV are mainly Al 3sp.

(iv) At around $E_F + 4$ eV, as a result of the interaction with Cu 3d states, a deep minimum is present in the Al 3p DOS and states appear to be almost quasipure Al 3p at about $E_F + 5.5$ eV; note that in this energy range the Al 3s curves which we report are modified because of the oxide contribution to the spectra.

(v) The high-lying states, from $E_F + 5.5$ eV to $E_F + 12$ eV are almost pure Al 3s.

On comparison with pure metals, these various interactions pull the Fe 3d states towards E_F by about 1.0 ± 0.2 eV while those belonging to Cu are pushed down deep in the band by about the same quantity i.e. 1.4 ± 0.2 eV (see table 5); the Cu and Fe 3d subbands are narrowed by about 1 eV; this is consistent with the lack of Cu or Fe first neighbours in the alloys. Mori *et al* (1991) have studied the valence band state distribution of I-Al$_{65}$Cu$_{21}$Fe$_{14}$ by photoemission spectroscopy measurements. They found a large peak at about 4 eV from E_F which they attributed to the presence of Cu 3d states. According to the experimental precision, this energy position is consistent with our own data.

The valence state distributions are found to be similar for all the other alloys which we have analysed whatever their structural state might be; as an example, figure 5 shows the result for D-Al$_{65.5}$Cu$_{18.5}$Fe$_8$Cr$_8$.

This indicates that the most important features of the DOS in all these materials are governed by the local order, i.e. by order arising from the chemical bond. Nevertheless, for our alloys, according to the atomic structure, the fine structure is somewhat different: as an example let us recall that the edges of the Al subbands are double in crystalline and decagonal alloys. This has been already observed for Al L$_{2,3}$ edges in C-Al–Mn or D-Al–Mn phases and was interpreted to result from
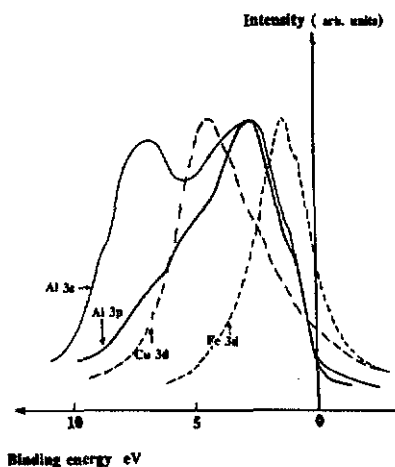
Figure 5. Al 3p (bold curve), Al 3s (thin curve), Fe 3d (short dashed curve) and Cu 3d (long dashed curve) state distribution curves in D-$Al_{65.5}Cu_{18.5}Fe_8Cr_8$ alloy.

the existence of long-range periodicity in the crystalline alloys and to the presence of a direction of symmetry in decagonal phases (Belin and Traverse 1991, Belin *et al* 1991). Also, from table 3, it arises that the intensity of the secondary peak of the Al 3p distribution, labelled B, is connected to the Cu concentration in the alloy. Indeed, peak B is well contrasted in C-Al–Cu–Fe phases and slightly less in the icosahedral phases, whereas it is hardly resolved in the Al–Cu–Fe–Cr alloys; the Cu concentrations decrease from the C-Al–Cu–Fe alloys to the Al–Cu–Fe–Cr alloys. Thus, the splitting of the Al 3p subband is attributed to the interaction of Al p states with the Cu 3d states. This suggests a Fano-like interaction similar to those studied by Terakura (1977) and Nguyen Manh *et al* (1985). It is thus surprising that our results do not provide similar experimental evidence in the Al 3s distribution; let us recall that oxidation modifies significantly the shape of the spectra at energies as low as $E_F + 4$ eV.

The binding energies of the Cu $2p_{3/2}$ and Fe $2p_{3/2}$ levels in the alloys are about 933.5 ± 0.3 eV and 706.5 ± 0.3 eV, respectively. According to the experimental uncertainties, this value is similar to that in the pure metal for Cu. On the other hand, we observe that the Al $2p_{3/2}$ level shifts by about 0.3–0.4 eV towards the oxide, revealing that Al acquires a slight ionic character. This suggests that in the alloys the interactions between the different metal states can be understood through a charge transfer which might originate from Al towards Fe and Cu orbitals and, as a consequence, tends to localize somewhat the different valence states. It follows that the free-electron model should not be invoked to analyse the electronic properties of these alloys; this agrees with previous conclusions concerning various quasicrystalline systems (see e.g. Wagner *et al* 1989, Phillips and Rabe 1991, Klein *et al* 1991, Cyrot-Lackmann *et al* 1991).

Note that Matsuo *et al* (1989) have studied magnetic properties and the electronic structure of a stable I-Al–Cu–Fe phase. They concluded that virtual bound 3d states must be located well below the Fermi level in the s and p bands. This is totally in contradiction to what we have observed experimentally and what is deduced from various theoretical calculations (see e.g. Fujiwara 1990, Cyrot-Lackmann *et al* 1991, Mayou 1991, Tramblay *et al* 1992).

According to the precision of the measurements, the Al 3sp DOS intensity at E_F for all the alloys is quite low and varies from one sample to another as reported

in table 3. The values tend to decrease slightly for a given structural state with increasing Al concentration which once more supports the non-validity of the free-electron model for these alloys. For I-$Al_{62}Cu_{25.5}Fe_{12.5}$, as a function of the more or less perfect structural quasicrystalline state, the DOS at E_F decreases a little. As reported previously, the Al 3sp DOS at E_F in a series of Al–Mn and Al–Mn–Si alloys, crystalline or quasicrystalline, is related to the value of their resistivity ρ: the higher the resistivity, the lower is the Al 3sp DOS at E_F (Belin and Traverse 1991, Belin *et al* 1991). Resistivity measurements have been performed on two I-Al–Cu–Fe phases almost identical to those reported in table 1. These measurements show that at 4 K, ρ is 1300 $\mu\Omega$ cm in the as quenched sample where it is 4300 $\mu\Omega$ cm in the annealed sample, i.e. a phase which is most structurally perfect (Klein *et al* 1990). This increase in resistivity is connected to the decrease that we observed in the sp DOS at E_F; thus, lower DOSS at E_F are expected for the I-$Al_{63}Cu_{25}Fe_{12}$ alloys for which resistivities as high as 11 000 $\mu\Omega$ cm have been measured recently (Klein *et al* 1991) and for which SXS measurements are in progress. On the other hand, Wagner *et al* (1989) reported that in stable I-Al–Cu–Fe quasicrystals, the DOSS at E_F are very low, as small as one sixth of their value in a free-electron model. They also reported that, for I-$Al_{65}Cu_{20}Fe_{15}$ samples, wide variations in ρ-values are seen from one sample to another. In view of our results, these variations could be attributed to differences in the structural quasicrystalline state, namely to the presence of different topological defects. Let us also mention that the low DOSS at E_F were deduced from specific heat measurements on various I-Al–Cu–Fe samples by Berger *et al* (1990).

The very high values of ρ that are observed for the Al–Cu–Fe alloys are also consistent with the presence of a pseudo-gap at E_F which is rather important and increases slightly from the decagonal to the icosahedral alloy. This pseudo-gap is also present in the related crystalline or microcrystalline counterparts but its value is lower. Such a pseudo-gap, but of smaller amplitude, has already been seen experimentally, e.g. in Al–Mn and Al–Mn–Si alloys (Belin and Traverse (1991) and references therein).

Pseudo-gaps in the electronic distributions have been predicted theoretically from various models e.g. by Fujiwara (1990) and Fujiwara and Yokokawa (1991) for Al–Mn, Al–Li–Cu and Al–Fe crystalline approximants of the quasicrystalline phases in an LMTO approximation.

The calculation of the valence DOSS in Al–Li and Al–Li–Cu alloys produces a band with a rounded shape when there is no Cu in the sample whereas, for the alloys containing Cu, there is a peak in the DOS at about 4–5 eV from E_F; this latter value is consistent with our data. Low DOSS are found at the Fermi level and Cu atoms do not seem to play a significant role in the formation of the pseudo-gap in the Al–Li–Cu alloys. For Al–Fe the calculation predicts a sharp maximum in the DOS at about 1.7 eV; partial DOSS are not given in this reference but, by analogy to Al–Mn (Fujiwara 1990), this structure can be ascribed to d states originating from Fe. In our samples, which contain Cu atoms, Fe 3d states are slightly closer to E_F than predicted by the calculation. This indicates that, in these alloys, Cu atoms could actually play a role more important than predicted, the result of which is to push the Fe states slightly towards the Fermi level, and to concentrate the Al 3sp DOS towards high energies; as a consequence the DOS at E_F is lowered and the stability enhanced by comparison with alloys such as Al–Mn for which Mn d states are found closer to E_F. This role of Cu d states will be investigated using D-Al–Mn–Cu and I-Al–Mn–Pd alloys and this study is in progress.

It is surprising that the result of alloying together good metals such as Al or Cu produces such high-resistivity materials. However, the phases that we have studied and other related phases, namely Al–Li–Cu and Al–Mg–Zn are not the only examples; other alloys may also exhibit high resistivity values. For example, Prekul (1978), Prekul and Sasovskaya (1979) and Schcherbakov *et al* (1983) invoke the existence of a pseudo-gap in the electronic structure to explain the high-resistivity properties of Ti-based alloys such as Ti–V or Ti–Nb, and Al_3Mn has been suggested to be a semiconductor (Kolomiets and Popova 1960).

4.2. Conduction state distributions

The curves showing the variation in empty p DOSs for pure Al, Fe and Cu (figure 3) are in accordance with theoretical calculations performed by Papaconstantopoulos (1986) using an SK LCAO model. For Al, at about 5 eV from the edge, the theoretical curve shows a peak denoted A. For Fe and Cu, just beyond the edge, the calculated curves exhibit a more or less sharp bump A, followed by a minimum B and an abrupt increase in intensity labelled C. Because of the broadening of the DOS by the lifetime of the core hole involved in the x-ray transition and the instrumental function, the increase C is smoothed out and thus appears to be more or less monotonic in the experimental curves.

For the $I\text{-}Al_{62}Cu_{25.5}Fe_{12.5}$ alloy, the distribution of the Al p empty states is a little modified in shape with respect to the metal and the edge is less abrupt. The edge of the empty Fe p state distribution has the same slope as in the metal while in the case of Cu the edge is less abrupt than in the metal. Both the Fe p and the Cu p distributions of $I\text{-}Al_{62}Cu_{25.5}Fe_{12.5}$ are less structured than those of the corresponding pure metals; in particular, minimum B is absent. All these observations suggest that, compared with the metals, modifications of hybridization take place in the quasicrystal which affect the p-state distribution slightly.

The three Al, Fe and Cu K curves normalized to their respective maximum intensity have been adjusted as mentioned above and the result is displayed in figure 6. It shows that in the conduction band the Al, Fe and Cu p states overlap each other.

Empty-state distributions of other symmetries are necessary to discuss more completely the conduction DOS. In particular, obtaining the Fe $L_{2,3}$ spectra would be very advantageous in ascertaining the possible charge transfer to Fe orbitals; indeed, the shape of the $L_{2,3}$ curve could be strongly modified if d states are more filled in the icosahedral alloy than in the pure metal. In fact, from preliminary experiments on an Al–Cu–Fe quasicrystal (Fuggle 1991), it seems that the photoabsorption intensity just beyond the edge, which arises from empty d states, is less contrasted in the quasicrystalline sample than in the pure metal. Complementary experiments will be considered in the near future.

We have plotted in figure 7 both the Al 3p and the Al p distribution curves for $I\text{-}Al_{62}Cu_{25.5}Fe_{12.5}$; this figure highlights the presence of a rather important pseudo-gap, about 1.6 eV, in the Al state distribution of the Al–Cu–Fe alloys. This observation of a wide pseudo-gap with the Fermi level lying in it supports the idea that the high stability of the $I\text{-}Al_{62}Cu_{25.5}Fe_{12.5}$ quasicrystal could be attributable to Hume-Rothery behaviour. The same could be true for the related crystalline phases, but owing to the higher intensity at the Fermi level the stability is expected to be less strong than for the quasicrystal. A similar interpretation is expected to be valid for Al–Cu–Fe–Cr alloys. Further experiments on the Al K spectrum are in progress.
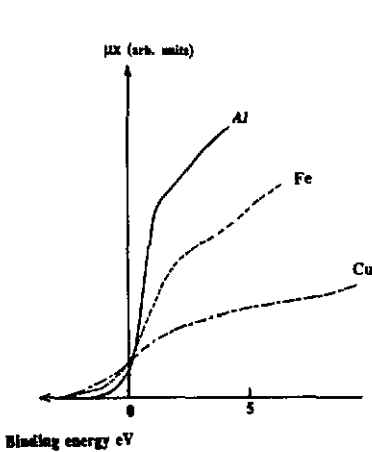
Figure 6. Al (bold curve), Fe (dashed curve) and Cu (chain curve) p conduction state distributions for I-$Al_{62}Cu_{25.5}Fe_{12.5}$ alloy.
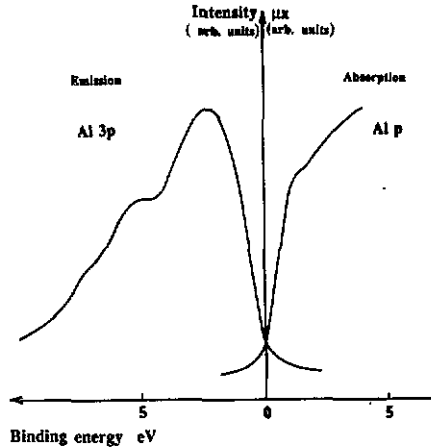
Figure 7. Valence Al 3p and conduction Al p state distribution for I-$Al_{62}Cu_{25.5}Fe_{12.5}$ alloy.

5. Conclusion

This paper reports on the analysis by SXES and SXAS experiments of valence and p conduction state distributions in various Al–Cu–Fe and Al–Cu–Fe–Cr alloys.

We have analysed the electronic interactions taking place between Al 3sp states and Cu and Fe d states of the valence band and suggest that its arrangement is due to a little charge transfer from Al towards Fe and Cu orbitals. The Al–Cu interaction tends to reinforce the p character of the Al 3p states of the middle of the band which seem to be isolated and makes the free-electron model not suitable for explaining the electronic properties of the Al–Cu–Fe and Al–Cu–Fe–Cr alloys.

The Al DOSS at E_F are found to be quite low. They are a little lower in the quasicrystals than in the crystalline phases. In the icosahedral samples, the DOS at E_F is lowered by improving the structural purity. The low DOSS at E_F are related to the high resistivity values which are observed for the icosahedral alloys.

A salient observation is the occurrence of a rather wide pseudo-gap at E_F, with the Fermi level lying approximately in the middle. Although this pseudo-gap is found to be wider in the quasicrystalline phases, it is also present in their crystalline counterparts or in crystalline phases of different nominal compositions.

Acknowledgments

References

Belin E, Kojnok J, Sadoc A, Traverse A, Harmelin M, Berger C and Dubois J M 1991 *J. Phys.: Condens. Matter* **4** 1057

Belin E and Traverse A 1991 *J. Phys.: Condens. Matter* **3** 2157

Berger C, Gozlan A, Lasjaunias J C, Fourcaudot G and Cyrot-Lackmann F 1991 *Phys. Scr.* **35** 90

Bessière M, Quivy A, Lefebvre S, Devaud-Rzepski J and Calvayrac Y 1991 *J. Physique* **1** 1823

Biggs B D, Poon S J and Munirathman N R 1990 *Phys. Rev. Lett.* **65** 2700

Briggs D and Seah M P 1983 *Practical Surface Analysis by Auger and X-ray Photoelectron Spectroscopy* (New York: Wiley) p 484

Calvayrac Y, Quivy A, Bessière M, Lefebvre S, Cornier-Quiquandon M and Gratias D 1990 *J. Physique* **51** 417

Cyrot-Lackmann F, Berger C, Gozlan A, Klein T and Mayou D 1991 *Proc. Int. Symp. on the Physics and Chemistry of Finite Systems: from Cluster to Crystal (Richmond)* at press

Dong C and Dubois J M 1991 *J. Mater. Sci.* **26** 1647

Fuggle J C 1991 private communication

Fujiwara T 1990 *J. Non-Cryst. Solids* **117–8** 844

Fujiwara T and Yokokawa T 1991 *Phys. Rev. Lett.* **66** 333

Kimura K 1991 *Mater. Sci. Eng.* A **133** 94

Kimura K, Kishi K, Hashimoto T, Takeuchi S and Shibuya T 1991 *Solid State Phys. (Japan)* **26** 501

Klein T, Gozlan A, Berger C, Cyrot-Lackmann F, Calvayrac Y and Quivy A 1990 *Europhys. Lett.* **13** 129

Klein T, Berger C, Mayou D and Cyrot-Lackmann F 1991 *Phys. Rev. Lett.* **66** 2907

Kolomiets N V and Popova E A 1960 *Fiz. Tverd. Tela* **2** 1951

Matsuo S, Nakano H, Ishimasa T and Fukano Y 1989 *J. Phys.: Condens. Matter* **3** 6893

Mayou D 1991 private communication

Mori M, Matsuo S, Ishimasa T, Matsuura T, Kamiya K, Inokuchi H and Matsukawa T 1991 *J. Phys.: Condens. Matter* **3** 767

Nguyen Manh D, Mayou D, Pasturel A and Cyrot-Lackmann F 1985 *J. Phys. F: Met. Phys.* **15** 1911

Papaconstantopoúlos D 1986 *Handbook of the Band Structure of Elemental Solids* (New York: Plenum) pp 208, 102, 122

Phillips J C and Rabe K M 1991 *Phys. Rev. Lett.* **66** 923

Prekul A F 1978 *Phys. Lett.* **64A** 473

Prekul A F and Sasovskaya I I 1979 *Solid State Commun.* **30** 91

Sadoc A, Flank A M and Lagarde P 1991 *X-ray Absorption Fine Structure* ed S S Hasnain (Chichester, West Sussex: Ellis Horwood) p 536

Schcherbakov A S, Prekul A F and Pomortsev R V 1983 *Phil. Mag.* B **47** 63

Smith A P and Ashcroft N W 1987 *Phys. Rev. Lett.* **59** 1365

Terakura K 1977 *J. Phys. F: Met. Phys.* **7** 1773

Tramblay G, Nguyen Manh D and Mayou D 1992 unpublished

Traverse A, Dumoulin L, Belin E and Sénémaud C 1988 *Quasicrystalline Materials (Institut Laue–Langevin CODEST Workshop)* ed C Janot and J M Dubois (Singapore: World Scientific) p 399

Wagner J L, Wong K M and Poon S J 1989 *Phys. Rev.* B **39** 8091